OUKA
The University of Osaka
Institutional Knowledge Archive

Title	Knitted and cross-linked elastomers for tough and removable pressure sensitive adhesives enabling stretch-induced debonding
Author(s)	Kosaba, Sho; Yamaoka, Kenji; Ikura, Ryohei et al.
Citation	Chemical Engineering Journal. 2026, 527, p. 171633
Version Type	VoR
URL	https://hdl.handle.net/11094/104011
rights	This article is licensed under a Creative Commons Attribution 4.0 International License.
Note	

The University of Osaka Institutional Knowledge Archive : OUKA

https://ir.library.osaka-u.ac.jp/

The University of Osaka

Chemical Engineering Journal 527 (2026) 171633



Contents lists available at ScienceDirect

Chemical Engineering Journal

journal homepage: www.elsevier.com/locate/cej





Knitted and cross-linked elastomers for tough and removable pressure sensitive adhesives enabling stretch-induced debonding

Sho Kosaba [a,b], Kenji Yamaoka [a,c], Ryohei Ikura [a,c], Takayuki Arai [b], Yoshinori Takashima [a,c,d,*]

[a] Department of Macromolecular Science, Graduate School of Science, The University of Osaka, 1-1 Machikaneyama, Toyonaka, Osaka, 560-0043, Japan
[b] LINTEC Corporation, 5-14-42, Nishiki, Warabi, Saitama, 335-0005, Japan
[c] Forefront Research Center (FRC), The University of Osaka, 1-1 Machikaneyama, Toyonaka, Osaka, 560-0043, Japan
[d] Institute for Open and Transdisciplinary Research Initiatives (OTRI), The University of Osaka, 2-1 Yamadaoka, Suita, Osaka, 565-0871, Japan

ARTICLE INFO

Keywords:
Tough elastomer
Sustainable chemistry
Pressure sensitive adhesive
Materials science
Debonding

ABSTRACT

Optically transparent pressure-sensitive adhesive (PSA) sheets are widely used in display technologies, where high optical clarity and low haze are essential. Beyond transparency, these PSA sheets must also exhibit reliable adhesion and the ability to follow surface irregularities. While soft and flexible materials typically accommodate uneven surfaces well, they often suffer from poor adhesive reliability or insufficient creep resistance post-lamination. In this study, we developed a knitted polymer (KP) elastomer that achieves a balance between step-following ability and mechanical durability. The KP elastomer is composed of a primary polymer grafted with cyclodextrins (CDs), and a second polymer that penetrates the cavities of CDs. Additionally, aluminum ions form chelate cross-links within the second polymer network, enhancing its structural integrity. This dual-network architecture imparts both step-following ability through movable cross-linking and creep resistance via aluminum chelate cross-linking. The elastomer also demonstrates mechanical robustness, allowing for stretch-induced debonding through simple stretching. Furthermore, the PSA sheet can be fully removed from substrates by dissolution in an appropriate solvent. This work presents an innovative PSA system that supports the circular use of display components and addresses emerging needs in advanced display manufacturing.

1. Introduction

Optically transparent adhesive sheets are indispensable components in modern display technologies, including televisions, smartphones, automotive displays, and wearable devices [1–9]. As displays evolve toward thinner and larger formats [10], adhesives must maintain their ability to follow surface topographies such as ink steps, touch sensor wiring, printed circuits, semiconductor elements, and contaminating dust [1,11]. These ink steps typically range from 0.1 to 10 μm in height and must be embedded by an adhesive layer with a thickness of up to 1 mm [12]. Adhesive materials for these applications are commonly categorized into liquid adhesives and elastomeric pressure-sensitive adhesive (PSA) sheets. While liquid adhesives offer superior wetting and step-following capabilities, their handling poses challenges due to flowability and volume shrinkage upon curing. In contrast, PSA sheets offer advantages in terms of ease of cutting, alignment, and bonding, but often exhibit insufficient step-following capabilities [10,12].

Various PSA chemistries have been explored, including acrylics, epoxies, natural rubbers, silicones, and urethanes [3,6,13–20]. Among these, acrylic-based PSAs are particularly well suited for optical applications due to their high transparency, tunable properties, and cost-effectiveness [9,14,21,22]. Conventional design strategies for acrylic PSAs involve light cross-linking of low-glass-transition-temperature (T_g) polymers to maintain tack and followability [12,23]. However, minimal cross-linking often compromises adhesion durability and creep resistance. Therefore, PSAs for display applications must achieve a delicate balance between softness (to embed ink steps) and mechanical toughness (to resist creep deformation) [10]. Additionally, given the high cost and functionality of display components, these adhesives must be removable to allow for recovery and reuse of valuable parts [4,7,10,24]. As such, current research is focused on developing PSAs that combine reliable adhesion with controlled debonding [25–33].

In this study, we report a uniform PSA sheet that simultaneously exhibits high conformability and toughness. The key innovation lies in

* Corresponding author at: Department of Macromolecular Science, Graduate School of Science, The University of Osaka, 1-1 Machikaneyama, Toyonaka, Osaka, 560-0043, Japan.
E-mail addresses: ta-arai@post.lintec.co.jp (T. Arai), takasima@chem.sci.osaka-u.ac.jp (Y. Takashima).

https://doi.org/10.1016/j.cej.2025.171633
Received 7 June 2025; Received in revised form 27 November 2025; Accepted 5 December 2025
Available online 12 December 2025
1385-8947/© 2025 The Authors. Published by Elsevier B.V. This is an open access article under the CC BY license (http://creativecommons.org/licenses/by/4.0/).

the synergistic use of two types of non-covalent cross-links: aluminum chelate cross-linking and movable cross-linking. Aluminum-chelated networks are well established in both academic and industrial PSAs [34–39] and are now also employed in self-healing and shape-memory materials owing to their reversible coordination bonds [40,41]. Such cross-links form through interactions between mono- and multi-coordinated metal ions and carboxylate ligands [42]. We selected aluminum ions due to their strong complex-forming ability and commercial availability [40]. Movable cross-linking, on the other hand, has been extensively studied for its ability to enable stress dissipation and mechanical reinforcement in polymer networks [35,43–46]. Notable approaches include host–guest chemistry [47,48], polyrotaxane architectures [49,50], and cyclodextrin (CD)-based movable cross-linking [30,51,52]. In our previous work, we developed a knitted polymer (KP) system consisting of a primary CD-grafted polymer and a second polymer threaded into the CD cavities [43,53]. This architecture provided high elasticity and the ability to combine dissimilar polymers. In the present study, we synthesized a KP elastomer from poly(ethyl acrylate) and a copolymer comprising n-butyl acrylate (BA), methyl acrylate (MA), and acrylic acid (AAc). Movable cross-links were established through CD inclusion, while aluminum chelation was introduced via carboxylic acid groups. The resulting KP elastomer exhibits excellent adhesive performance, including peel strength, creep resistance, and step-following capabilities—even at high cross-link densities. Notably, KP-AC(10) allows for stretch-induced debonding and can be thermally remolded after removal. Furthermore, residues that remain on substrates can be readily dissolved in acetylacetone, ensuring complete removal.

Here, we present a robust, optically transparent PSA that offers both high performance and environmental compatibility. This system facilitates the reuse of substrates and enables adhesive recycling, addressing emerging needs in the advanced display industry (Fig. 1).

2. Results and discussion

2.1. Design strategy and preparation of the PSA

We synthesized a series of KP elastomers, along with several control samples, to investigate the effects of different cross-linking interactions on material properties and each chemical structure (Fig. 2). KP-AC(x) was designed as referenced in our previous work. Its recyclable, movable cross-linked PSA had 0.5 mol% of CD, and the theoretical T_g was about −26 °C. Within these constraints, we selected some monomers as a second polymer. MA was the hard segment and a small-radius monomer to promote the generation of movable cross-linking. BA was a soft polymer to provide the PSA wettability and superior adhesive property. AAc provided two functions: acting as the cross-linking site for aluminum chelation and imparting cohesiveness, as well as having a small radius. Scheme 1 illustrates the chemical structure of the aluminum-chelated KP elastomer, denoted as KP-AC(x). KP-AC(0), LP/EA-CD, KP-CC, and LP-AC were synthesized via bulk polymerization as detailed in Schemes S1–S4 and Fig. S3, using the composition ratios listed in Table 1. LP/EA-CD was prepared by mixing PEA-CD and LP-AC in acetylacetone, followed by solvent evaporation (Scheme S5).

2.2. Characterization of the structure and cross-linking

The resulting KP-AC(x) elastomers exhibited sufficient optical clarity for use as transparent PSAs (Table S2). Characterization of aluminum chelate cross-linked elastomers by techniques such as GPC and ^{1}H NMR proved difficult due to limited solubility. Therefore, structural analysis was primarily conducted on KP-AC(0), a representative sample lacking aluminum cross-links, which could be dissolved in organic solvents such as $CDCl_3$ for ^{1}H NMR and tetrahydrofuran for GPC (Figs. S3–S5). The composition ratio of KP-AC(0) was confirmed by integrating the peak areas in the ^{1}H NMR spectrum, indicating that all precursor components remained intact after the drying process. FT-IR analysis showed the disappearance of vinyl C=C bending vibrations, confirming removal of residual monomers (Fig. S7b). GPC analysis revealed a weight-average molecular weight (M_w) of 230 kDa for KP-AC(0), compared to 145 kDa for PEA-CD, suggesting that the second polymer had a higher molecular weight than the CD-grafted polymer (Fig. S5).

Cross-linking was further validated using various analytical techniques for both movable and aluminum chelate cross-links. The existence of movable cross-links was supported by 2D-NOESY spectroscopy and rheological measurements. In the 2D-NOESY spectrum, a model

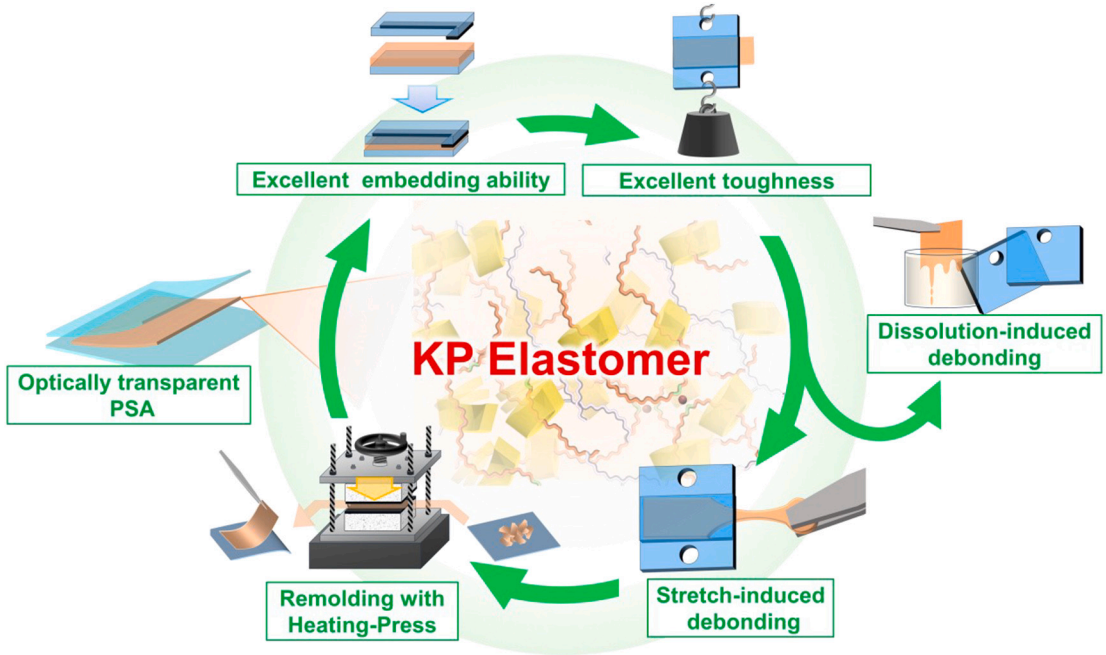


Fig. 1. Conceptual illustration of the multifunctional adhesion elastomer developed in this study. The KP elastomer can embed ink steps or surface irregularities, resist creep, undergo stretch-induced debonding for removal from substrates, be remolded via thermal pressing, and be dissolved in specific solvents.

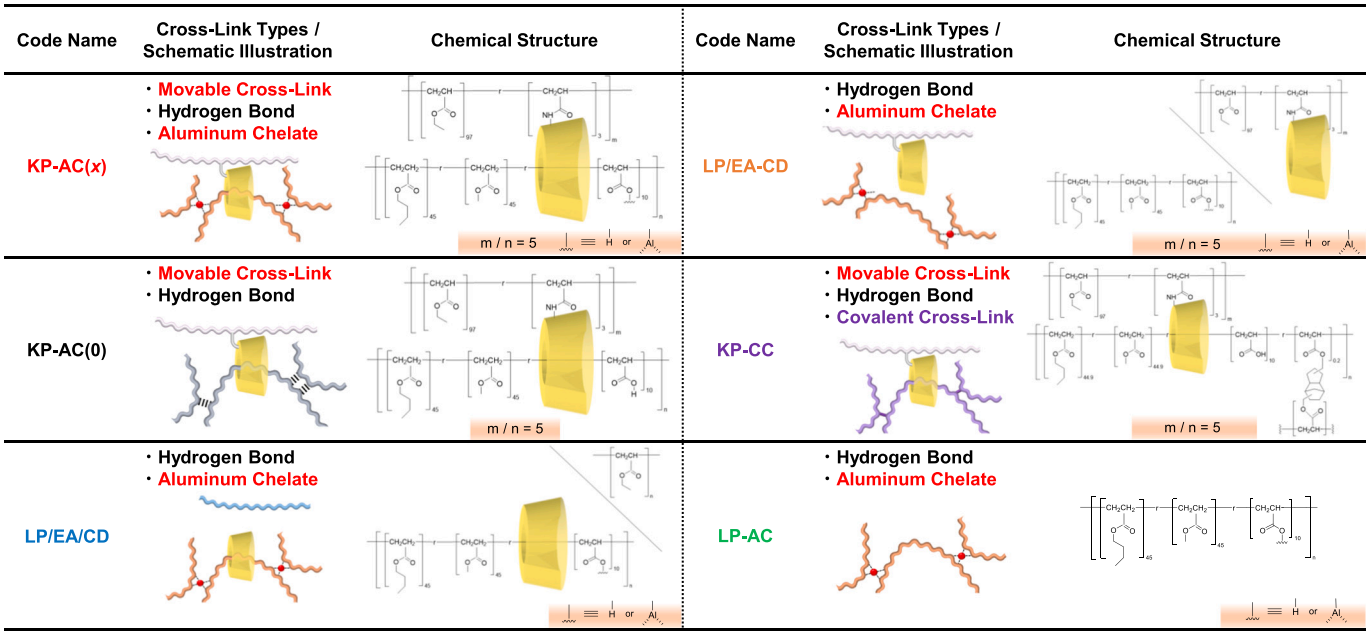
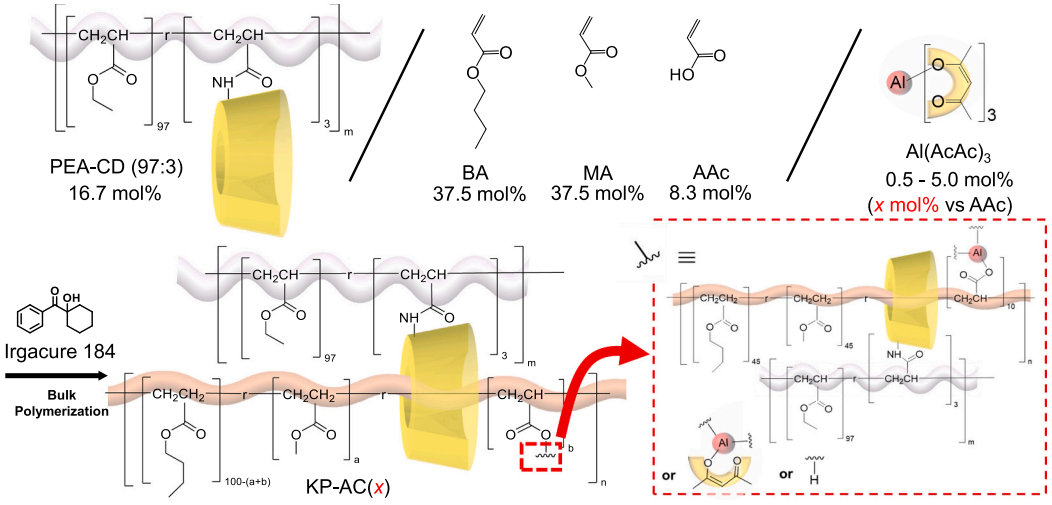


Fig. 2. Schematic illustrations and chemical structures of each elastomer and the key intermolecular interactions investigated in this study.



Scheme 1. Preparation of KP-AC(*x*). A mixture of monomers, polymer, photoinitiator, and cross-linker was bulk-copolymerized under UV irradiation (λ = 365 nm, 0.1 W/cm^2, 5 J/cm^2), resulting in a network incorporating the PEA-CD polymer and a second polymer component.

Table 1
Compositions of acrylic elastomers.

Sample	1st Polymer		2nd Polymer			Cross-Linker			
	EA	TAcβCDAAm	MA	BA	AAc	$Al(AcAc)_3$	**Al^{3+} mol% / vs AAc**	A-DCP	Irg. 184
KP-AC(0)	16.0	0.5	37.5	37.5	8.5	-	**0**		0.2
KP-AC(1)	16.0	0.5	37.5	37.5	8.5	0.1	**1**		0.2
KP-AC(2)	16.0	0.5	37.5	37.5	8.5	0.2	**2**		0.2
KP-AC(5)	16.0	0.5	37.5	37.5	8.5	0.4	**5**		0.2
KP-AC(10)	16.0	0.5	37.5	37.5	8.5	0.8	**10**		0.2
LP/EA-CD	16.0	0.5	37.5	37.5	8.5	0.8	**10**		0.2
LP/EA/CD	16.0	0.5	37.5	37.5	8.5	0.8	**10**		0.2
KP-CC	16.0	0.5	37.5	37.5	8.5	-	**-**	0.2	0.2
LP-AC	-	-	45.0	45.0	10.0	1.0	**10**		0.2

compound showed proximity between the inner protons C(3) and C(5) of the CD cavity and the protons on the acrylic polymer backbone (Fig. S7a). However, those correlation peaks were absent in the spectrum of PEA-CD alone (Fig. S7b). These results explain that a simple copolymer with CD does not exhibit the correlation peaks with the inner protons of CD. Therefore, the secondary polymer after bulk polymerization would be included within the CD cavities. Rheological analysis of KP-AC(0)—which lacks any covalent or aluminum chelate cross-linkers—exhibited a deviation from the expected slope of 2 in the storage modulus (G') at low frequencies (Fig. S8), consistent with the presence of movable cross-linking.

Introduction of aluminum or diacrylate cross-linkers led to a further reduction in slope, suggesting enhanced network formation. FT-IR spectroscopy provided additional evidence for aluminum coordination, with increasing absorption intensity in the 1660–1512 cm^{-1} region as the aluminum content (x) increased in KP-AC(x). Furthermore, peak analysis after deconvolution showed a decrease in the intensity of the initial carbonyl peak, and an increase in the intensity of peaks shifted toward the low-wavenumber with increasing the amount of aluminum chelate (Fig. S6c–f). This change was due to the deprotonation of carboxylic acid by adding aluminum ions, then the peak of C═O stretching from carboxylate ion in the low wavenumber region compared to C═O from carboxylic acid such as around 1600 cm^{-1} or 1550 cm^{-1}. In contrast, KP-AC(10), which lacked acrylic acid units, showed minimal change in this region, similar to KP-AC(0), confirming the essential role of carboxylic acid groups in aluminum chelate cross-linking. Gel fraction analysis supported these findings: gel content after immersing in ethyl acetate increased with increasing x mol% (Fig. S9). Taken together, these results confirm that the KP-AC(x) elastomers incorporate at least two distinct types of cross-linking: movable cross-links formed via cyclodextrin and aluminum chelate cross-linking coordinated with carboxylate groups.

2.3. Adhesion properties of KP elastomers

The adhesive performance of the KP elastomers was evaluated using 180° peel tests, lap-shear tests, and creep resistance measurements. Each elastomer was laminated onto a polyethylene terephthalate (PET) film substrate and bonded to a soda-lime glass surface (Fig. 3a). After aging for 24 h, the PET film was peeled at an angle of 180°. As shown in Fig. 3b, all KP elastomers exhibited high peel strength. This trend is attributed to the balance between interfacial adhesion and internal deformation resistance during peeling. As indicated in the gel fraction, the chelate cross-linking density increases with x, the material's ability to adhere to the interface decreases. This phenomenon is supported by *Dahlquist* criterion, which states that tackiness decreases when the storage modulus (G') exceeds 0.3 MPa at the application temperature. Temperature-dependent G' measurements showed that increasing aluminum cross-linking reduced interfacial adhesion, consistent with the observed decrease in peel strength (Table S4, Fig. S10a and b). In contrast, the effective cross-linking density ν_e showed no dramatic change in KP-AC(x) elastomers (Table S4). This suggests that movable cross-linking and hydrogen bonds also work as effective cross-linking. Also, the superior peel strength of elastomers was explained by superior toughness, too. Elastomers were confirmed high toughness thanks to strain-hardening (Fig. S11). Notably, all KP elastomers showed significantly higher peel strength than LP-AC, a control elastomer lacking the CD-grafted primary polymer. Although LP-AC exhibited G' values indicative of sufficient tackiness [54], its mechanical resistance to deformation under peeling stress was lower than that of the KP elastomers. This would be related to high crosslinking density, so that too high cross-linking density may prevent the stress dispersion in the process of peeling. This result highlights the KP architecture's contribution to interfacial adhesion and cohesive strength.

The lap-shear tests were performed using the same PET substrate and

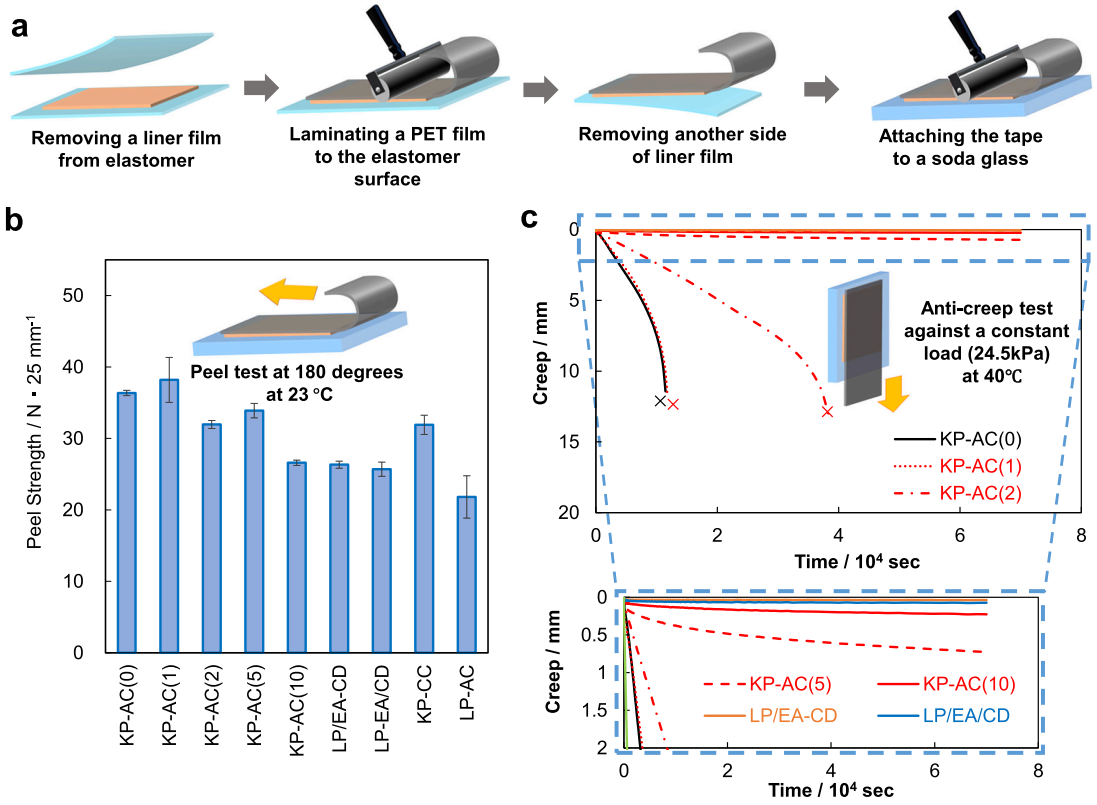


Fig. 3. Procedures for measuring the adhesive properties of the elastomers. (a) The elastomer was laminated with a PET film and adhered to soda glass. (b) Peel strength was evaluated by folding the PET film and pulling it at a 180° angle at 25 °C. (c) Creep resistance was assessed by pulling the PET film under a constant load of 24.5 kPa at 40 °C. This strain (~20 mm) is equal to 28,000 % strain versus the thickness of the elastomers.

glass adherent. KP-AC(x) showed the same tendency as peel tests (Fig. S13). Most samples exhibited interfacial failure in lap-shear tests, excluding LP/EA/CD, which contained free CD. Notably, the debonding interface was between glass and elastomers in peel tests, but it was between PET and elastomer in the lap-shear test.

Creep resistance was assessed by applying a vertical stress of 24.5 kPa at 40 °C and monitoring displacement over 70,000 s. As shown in Fig. 3c, creep resistance improved significantly for KP elastomers containing 2.5 mol% or more aluminum ions. Despite maintaining adequate tackiness at 40 °C, the improved creep behavior is attributed to enhanced network integrity. Regardless of whether movable cross-links were present, the incorporation of aluminum chelate cross-linking consistently conferred superior creep resistance. Importantly, the combination of aluminum chelate and movable cross-linking effectively addressed the intrinsic creep limitation observed in previously reported movable cross-linked systems [51]. This dual cross-linking strategy offers a promising approach to simultaneously achieving high peel strength and long-term reliability in optically transparent PSAs.

2.4. The ability to follow and embed ink steps

The ability of KP elastomers to follow surface irregularities was evaluated by embedding ink steps printed on soda-lime glass. Each elastomer was laminated onto a PET film, and the composite tape was then bonded over the ink steps (Fig. 4a). The degree of followability was quantified using the "Following Ratio", defined as the maximum height of the embedded step relative to the thickness of the elastomer (Eq. (1)):

$$\text{Following Ratio}\ (\%) = \frac{\text{Maximum embedded step height}\ (\mu\text{m})}{\text{Elastomer thickness}\ \ (\mu\text{m})} \times 100 \tag{1}$$

Optical microscopy images after lamination are shown in Fig. 4b. KP-AC(0), which lacks aluminum cross-linking, successfully embedded the ink steps under all tested conditions. In contrast, LP/EA-CD (a mixture of the primary polymer and a cross-linked secondary polymer) and LP-AC (only cross-linked second polymer) failed to embed even under the most favorable conditions. Remarkably, KP-AC(10)—despite containing the highest amount of cross-linkers—achieved a following ratio of 7–14 %. The only structural difference between KP-AC(10) and LP/EA-CD is the inclusion of the second polymer within the CD cavities of the primary polymer. This finding suggests that KP elastomers possess superior stress-relaxation and strain-dissipation capabilities, likely due to the dynamic behavior of the movable cross-links.

2.5. Stress relaxation behavior

To further investigate the stress relaxation capability of the elastomers, torsional shear tests were conducted. A 10 % instantaneous shear strain was applied, and the stress decay was recorded over 10,800 s (Fig. S14). The relaxation curves were fitted using the *Kohlrausch–Williams–Watts* (KWW) model, assuming two relaxation components and a permanent stress contribution (Eq. (2)).

$$\sigma(t) = \sum \sigma_r \exp\left\{ -\left(\frac{t}{\tau}\right)^{\beta} \right\} + \sigma_\infty \tag{2}$$

where σ_r is the relaxable stress, σ_∞ is the residual stress, τ is the time constant, and β is the stretching exponent.

The fitting parameters are summarized in Table 2, and all models demonstrated high correlation coefficients with the experimental data

Table 2
Fitting parameters for stress relaxation curves of elastomers in the KWW equation.

	σ_{r1}			σ_{r2}			$\sigma\infty/\sigma_0$	R^2
	σ_r/σ_0	τ/s	β	σ_r/σ_0	τ/s	β		
KP-AC(0)	0.58	0.03	0.33	0.42	0.87	0.16	0.00	0.999
KP-AC(2)	0.67	0.06	0.33	0.33	4.11	0.16	0.00	0.987
KP-AC(5)	0.63	0.03	0.33	0.34	1.46	0.16	0.03	0.984
KP-AC(10)	0.64	0.03	0.33	0.32	1.96	0.16	0.04	0.999
LP/EA-CD	0.52	0.05	0.33	0.39	1.88	0.16	0.09	0.989
LP/EA/CD	0.45	0.05	0.33	0.54	10.07	0.16	0.01	0.992
KP-CC	0.64	0.04	0.33	0.30	2.21	0.16	0.06	0.985
LP-AC	0.26	0.28	0.33	0.54	78.78	0.16	0.20	0.997

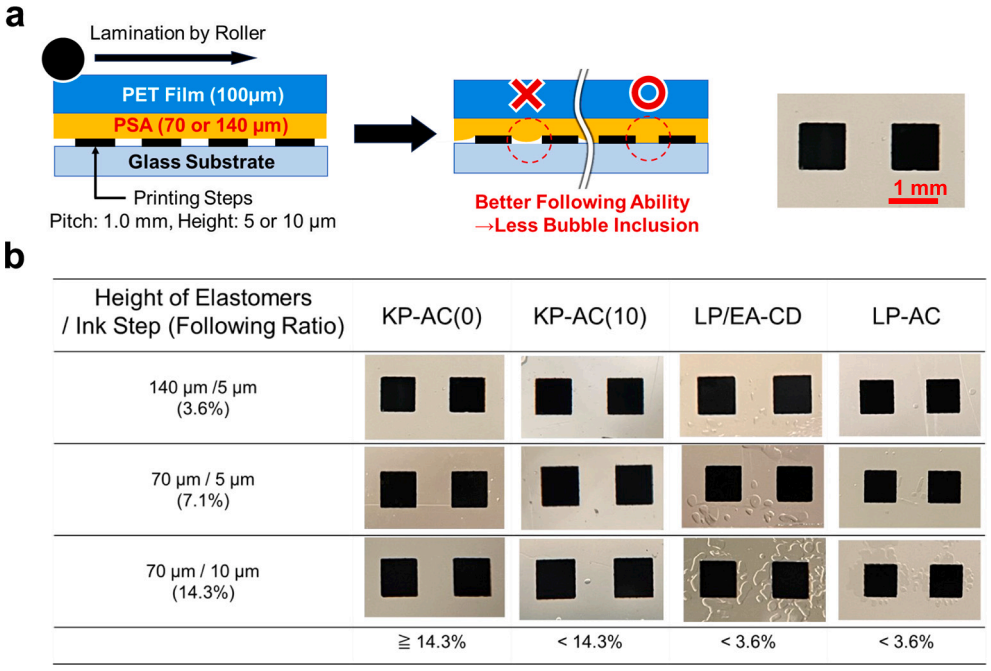


Fig. 4. Step-following test of the elastomers. (a) The elastomer, backed with a PET film, was laminated onto a glass substrate using a roller. Bubble inclusion was then examined from the side of the glass substrate using an optical microscope. (b) Optical microscope images of the elastomers after the step-following test. The threshold for bubble inclusion was determined based on the lowest condition at which bubbles were observed.

(Fig. S15a–h). A marked difference was observed in the initial relaxation phase (within 1 s) between elastomers containing CDs and those without. This suggests that the presence of bulky CD moieties facilitates rapid, large-segment mobility within the polymer network [55]. This phenomenon was further supported by the fitting results, where the CD-containing elastomers exhibited a higher proportion of the fast relaxation component and shorter relaxation times.

Focusing specifically on the fast component (σr1) in the stress relaxation test, the relaxation ratio (σr/σ0) was large for samples containing a KP structure. Even in the system with CDs, the ratio remained relatively small if the KP structure was absent. Particularly in LP-AC without CD, the fast component (σr1) ratio was clearly lower, and the relaxation time was relatively long. When comparing KP elastomers to LP/EA-CD and LP/EA/CD—both lacking movable cross-linking—the KP systems showed a more pronounced and efficient stress decay within the initial time window. In addition, the minimal residual stress observed in KP-AC(0) indicates that the persistent stress component is mainly associated with aluminum coordination bonds, rather than with the movable cross-links. These results suggest that the presence of CD molecules facilitates the rapid relaxation, an effect that is particularly

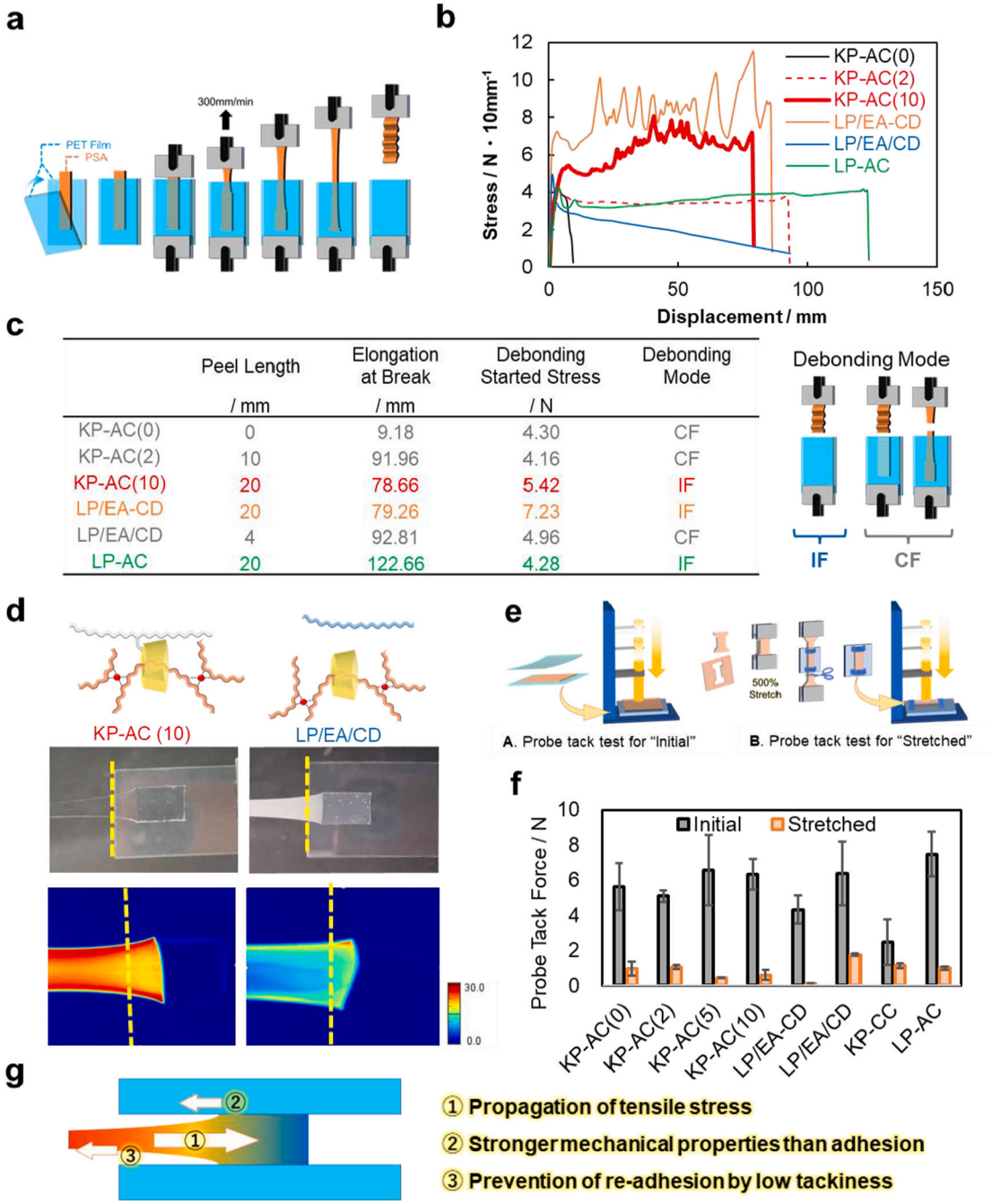


Fig. 5. Results of the stretch-induced debonding tests. (a) Each elastomer was laminated between PET films and stretched at a tensile speed of 300 mm/min until complete debonding. (b) Stress–strain curves recorded during debonding. (c) Summary of the stretch-induced debonding test results. Complete debonding was observed only for KP-AC(10), LP/EA-CD, and LP-AC. (d) Photographs and 2D birefringence images of KP-AC(10) and LP/EA/CD during debonding from a triacetylcellulose film. Yellow dashed lines indicate the edges of each adherent film. (e) Schematic of the probe tack test. "Initial" samples refer to the pristine elastomers, while "Stretched" samples were measured after 500 % uniaxial elongation. (f) Probe tack test results comparing initial and stretched conditions. (g) Proposed mechanism of stretch-induced debonding in pressure-sensitive adhesives (PSAs).

pronounced when a penetrated structure is present. Collectively, these results indicate that the high step-following ability of KP elastomers arises from two key mechanisms:

1. Rapid segmental relaxation, facilitated by the steric and dynamic nature of CD molecules, and
2. Efficient stress dissipation, enabled by the movable cross-linking network, which leaves minimal residual stress. Thus, CD-based movable cross-links play a critical role in enabling elastomers to embed ink steps.

2.6. Stretch-induced debonding behavior of KP elastomers

To evaluate the removability of KP elastomers from adherents, a stretch-induced debonding test was performed. In preliminary peel tests, the elastomers adhered more strongly to PET films than to glass substrates. Therefore, PET films were selected as the adherent, and the elastomer samples were sandwiched between two PET sheets. The removal length was recorded while stretching the specimen at a constant speed of 300 mm/min (Fig. 5a and b). All three elastomers—KP-AC(10), LP/EA-CD, and LP-AC—were completely removed by stretching (Fig. 5c). Among them, KP-AC(10) required lower force and shorter displacement for complete removal. According to prior literature [56–60], this form of clean removal is enabled by sufficient toughness to overcome interfacial adhesion. By uniaxial elongation of PSA layer, stress concentration near the frontal edge of the delamination occurs extremely and locally, initiating fracture at the interface. Adhesive tape can be removed from the substrate by stretching the tape in the direction of the flat surface of the bonded area, causing the adhesive to elongate and lose its tack. Following these steps, the polymer chains orient during elongation, and intermolecular forces with the substrate weaken; continuous delamination progresses. Additionally, strain-hardening of those elastomers would help the debonding process. The combination of movable and aluminum chelate cross-linking likely contributes to the mechanical toughness of KP-AC(10). Also, the debonding interface was different between the case of the peel test and the lap-shear test, which suggests stretch-induced debonding has a mechanism similar to shear debonding. Interestingly, in-situ observation using two-dimensional birefringence revealed that KP-AC(10) exhibited strong stress-induced birefringence during stretching, which propagated throughout the contact area between the elastomer and the adherent. In contrast, no birefringence was observed for LP/EA/CD, which has no knitting structure and failed to debond under similar conditions (Fig. 5d). This suggests that effective stress propagation—potentially due to polymer chain orientation—is a key factor in enabling stretch-induced debonding. The orientation of polymer chains during uniaxial elongation appears to enhance toughness, allowing the elastomer to overcome interfacial adhesion without fracturing. Despite having similar peel strengths, KP-AC(10) and LP/EA/CD showed markedly different debonding behaviors, highlighting the importance of stress distribution and internal stress dissipation mechanisms. Additional probe tack measurements under stretched and unstretched conditions were conducted (Fig. 5e). A significant reduction in tackiness upon stretching was observed in KP-AC(10), which is critical to prevent re-adhesion during debonding (Fig. 5f) [57,61–63]. As the tack decreased upon stretching, KP-AC(x) could be removed over a wider area by stretch-induced debonding. Also, it suggested that successfully debonding would be achieved in a shorter elongation (Figs. S11a and b). From these results, three criteria were identified as essential for achieving complete stretch-induced debonding (Fig. 5g):

1. Efficient stress propagation through the elastomer during elongation.
2. High mechanical toughness, allowing the elastomer to remain intact under stress exceeding interfacial adhesion.
3. Reduction of tackiness under strain, preventing re-adhesion during the debonding process.

2.7. Mechanical properties and their role in debonding behavior

To further understand the correlation between mechanical properties and stretch-induced debonding, the results of uniaxial tensile tests were observed in detail. KP-AC(x) elastomers exhibited a distinct plateau in the low-strain region (Fig. S12a), with the plateau length decreasing as x mol% increased. This plateau behavior is characteristic of stress dissipation via movable cross-linking. The decrease in plateau length with increasing x suggests that the mobility of CD moieties along the polymer backbone is restricted by higher cross-link density. LP/EA-CD, which lacks movable cross-linking, exhibited minimal plateau behavior (Fig. S12b). KP-CC, a covalently cross-linked version of the second polymer, followed a similar stress–strain curve as KP-AC(10) up to 500 % strain, but showed substantially lower elongation at break. This indicates that the aluminum chelate cross-links may undergo dynamic rearrangement under applied stress, contributing to toughness and extensibility.

Notably, the three elastomers that demonstrated complete debonding—KP-AC(10), LP/EA-CD, and LP-AC—also exhibited relatively high toughness (Table S5). Furthermore, KP-AC(10) and LP/EA-CD, which showed large changes in probe tack behavior at 500 % strain, also displayed significant differences in tensile stress between the unstretched and stretched states. In contrast, KP-AC(0) and LP/EA/CD, lacking aluminum and movable cross-linking, respectively, showed low stress levels at 500 % strain and minimal changes in tack.

These mechanical insights underscore the importance of both cross-linking design and dynamic stress response in enabling stretch-induced debonding. KP-AC(10), in particular, demonstrates the optimal balance of toughness, stress transferability, and dynamic surface properties required for high-performance debondable PSAs.

2.8. Recyclability and dissolution-induced debonding of KP elastomers

To evaluate the recyclability of KP-AC(10), removed elastomers were collected following stretch-induced debonding and reprocessed via hot-pressing at 150 °C under a load of 1 kN. The resulting films exhibited visual and mechanical properties comparable to those of the pristine material (Fig. 6a). Tensile tests and dynamic modulus measurements confirmed that the reprocessed elastomer retained its original elasticity and toughness (Fig. 6b). Although previous reports indicate that coordination exchange between aluminum ions and carboxylic acids typically occurs at over 160 °C [39], the applied pressure during hot-pressing likely acts as an external force that facilitates bond exchange even at the lower temperature. 150 °C is sufficiently higher than the T_g of the elastomers (Table S4). The data also suggest that both the aluminum chelate and the movable cross-links remain intact and undergo dynamic reorganization, preserving the original network architecture without significant degradation. The high elongation at break (~1400 %) further indicates that the material's structural integrity remains intact after reprocessing.

In addition to thermal reprocessing, KP-AC(10) elastomers exhibit selective solubility in coordination-active solvents. While the materials only swell in ethyl acetate—a common organic solvent—they dissolve completely upon exposure to acetylacetone, a β-diketone known to coordinate efficiently with aluminum ions. After ultrasonic treatment, a homogeneous solution was obtained, indicating full dissociation of the cross-linked network. The expansion of polymer chains differs significantly between dissolution and melting. The large expansion during dissolution contributes to the disassembly of KP structures. Therefore, reforming via dissolution permanently breaks KP structures. In contrast, during melting, rearrangement of the chelate bond would occur in the situation where the elastomer's volume does not change drastically. In this process, most KP structures do not undergo disassembly, resulting in post-reformation mechanical strength equivalent to virgin material, as shown in Fig. 6b. This difference in chain expansion would be the main cause of the recyclability gap.

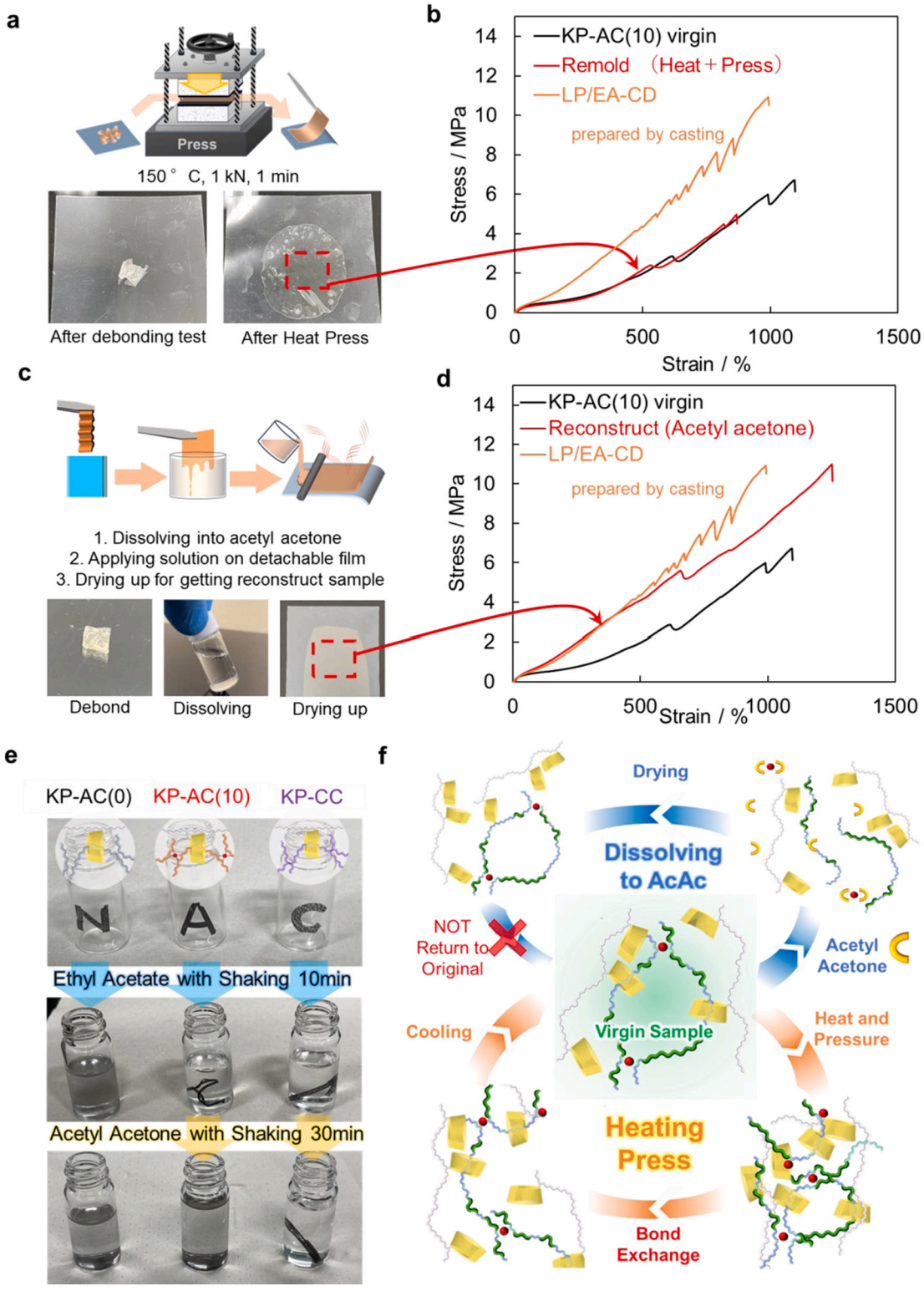


Fig. 6. Recyclability test of the KP-AC(10) elastomer sheet. (a) Process overview of KP-AC(10) remolding using a heating press. (b) Tensile test results of remolded KP-AC(10) compared to the virgin elastomer and LP/EA-CD. (c) Dissolution and reconstruction process of KP-AC(10) using acetylacetone. (d) Tensile test results of reconstructed KP-AC(10) compared to the virgin elastomer and LP/EA-CD. (e) Photographs from the solubility test. Three types of cross-linked elastomers were cut into alphabet shapes: N (no aluminum chelate, KP-AC(0)), A (aluminum chelate, KP-AC(10)), and C (covalent cross-linking, KP-CC). The elastomers were immersed in ethyl acetate and acetylacetone. Each elastomer was mixed with carbon black for visualization. (f) Schematic representation of the polymer structure during the remolding or reconstruction process.

Now, upon recoating this acetylacetone solution and drying, the resulting film displayed mechanical behavior similar to LP/EA-CD—a tough PSA lacking the movable cross-link architecture—suggesting that the PEA-CD and second polymer were fully dissociated during dissolution (Fig. 6c and d). This solvent-responsiveness highlights the versatility of KP-AC(x) systems: while maintaining high adhesion and creep resistance under normal conditions, the elastomers can be selectively disassembled either mechanically (via stretching) or chemically (via dissolution in acetylacetone). These properties are particularly advantageous in display technologies, where precise and clean removal of adhesives is essential for recovering expensive or delicate components (Figs. 6e and S9).

Overall, KP-AC(10) enables multimodal debonding, offering three distinct modes of removal and reuse:

1. Mechanical removal via stretch-induced debonding,
2. Thermal reprocessing through hot-pressing with complete property recovery, and
3. Solvent-based disassembly with selective dissolution of cross-links.

Remarkably, the reprocessed elastomer retains its original properties, and the dissolved network yields a functional PSA upon recoating. This demonstrates a rare combination of high performance and environmental compatibility, underscoring the potential of KP-AC(x) systems in sustainable display manufacturing and advanced adhesive technologies (Fig. 6f).

3. Conclusion

In conclusion, we successfully developed an optically transparent pressure-sensitive adhesive (PSA) sheet based on a KP elastomer architecture. By integrating cyclodextrin-based movable cross-linking with aluminum chelate cross-linking, the KP elastomer achieved a balance between step-following ability and mechanical durability.

This design enables excellent step-following capability, reliable adhesion, creep resistance, and mechanical robustness. Moreover, the PSA sheet exhibits stretch-responsive debonding and complete removability via solvent dissolution, aligning with the demands for reworkable and sustainable adhesive solutions in advanced display applications.

This work demonstrates the potential of supramolecular materials in creating next-generation PSAs that support circularity and functional integration in display technologies. To support the advancement and sustainability of modern optical devices, which have made rapid progress in recent years, we propose this multifunctional, eco-friendly, and transparent adhesive as a promising candidate for bonding optical functional components.

CRediT authorship contribution statement

Sho Kosaba: Writing – original draft, Methodology, Investigation, Funding acquisition, Formal analysis, Data curation, Conceptualization. **Kenji Yamaoka:** Writing – review & editing, Investigation. **Ryohei Ikura:** Writing – review & editing, Investigation. **Takayuki Arai:** Resources, Project administration, Conceptualization. **Yoshinori Takashima:** Supervision, Resources, Project administration, Conceptualization.

Declaration of competing interest

The authors declare that they have no known competing financial interests or personal relationships that could have appeared to influence the work reported in this paper.

Acknowledgements

This research was funded by the JST Core Research for Evolutional Science and Technology (CREST) program JPMJCR22L4; the JST COI-NEXT program JPMJPF2218; Scientific Research on Innovative Areas JP19H05714 and JP19H05721 from the MEXT of Japan; the Asahi Glass Foundation; the Yazaki Memorial Foundation for Science and Technology (Y.T.); International Polyurethane Technology Foundation; Toyota Riken Scholar Program (R.I.); the Iketani Science and Technology Foundation, 0351026-A and 0361034-A (R.I. and K.Y.); and the Suzuki Foundation (K.Y.).

Appendix A. Supplementary data

Supplementary data to this article can be found online at https://doi.org/10.1016/j.cej.2025.171633.

Data availability

Data will be made available on request.

References

[1] K. Ding, V. Avrutin, N. Izyumskaya, Ü. Özgür, H. Morkoç, Micro-LEDs, a manufacturability perspective, Appl. Sci. (Switz.) 9 (2019), https://doi.org/10.3390/app9061206.
[2] S.-W. Lee, J.-W. Park, Y.-E. Kwon, S. Kim, H.-J. Kim, E.-A. Kim, H.-S. Woo, J. Swiderska, Optical properties and UV-curing behaviors of optically clear semi-interpenetrated structured acrylic pressure sensitive adhesives, Int. J. Adhes. Adhes. 38 (2012) 5–10, https://doi.org/10.1016/j.ijadhadh.2012.04.002.
[3] S.W. Lee, J.W. Park, C.H. Park, H.J. Kim, E.A. Kim, H.S. Woo, Optical properties and adhesion performance of optically clear acrylic pressure sensitive adhesives using chelate metal acetylacetonate, Int. J. Adhes. Adhes. 47 (2013) 21–25, https://doi.org/10.1016/j.ijadhadh.2013.09.006.
[4] Y.G. Kim, B.M. Park, J.K. Choi, D.H. Jang, K.Y. Han, Optimization of the rework of bended oled displays by surface-energy control, Coatings 11 (2021), https://doi.org/10.3390/coatings11121523.
[5] T.H. Lee, G.Y. Han, M.B. Yi, H.J. Kim, J.H. Lee, S. Kim, Rapid photoresponsive switchable pressure-sensitive adhesive containing azobenzene for the mini-light emitting diode transfer process, ACS Appl. Mater. Interfaces 13 (2021) 43364–43373, https://doi.org/10.1021/acsami.1c11680.
[6] C. Hwang, S. Shin, D. Ahn, H.J. Paik, W. Lee, Y. Yu, Realizing cross-linking-free acrylic pressure-sensitive adhesives with intensive chain entanglement through visible-light-mediated photoiniferter-reversible addition-fragmentation chain-transfer polymerization, ACS Appl. Mater. Interfaces 15 (2023) 58905–58916, https://doi.org/10.1021/acsami.3c15002.
[7] Y. Du, Y. Bai, W. Gao, L. Meng, Y. Bai, Research progress on displays and optical adhesives for flexible 3C products, Eur. Polym. J. 212 (2024) 113053, https://doi.org/10.1016/j.eurpolymj.2024.113053 (accessed March 13, 2025).
[8] M.-B. Yi, T.-H. Lee, S.-J. Lee, J.-S. Kim, H.-J. Kim, Topologically designed cross-linking network for stretchable and recoverable pressure-sensitive adhesives with exceptional softness, Mater. Today Chem. 26 (2022) 101141, https://doi.org/10.1016/j.mtchem.2022.101141.
[9] E.S. Kim, J.H. Lee, D.H. Suh, W.J. Choi, Influence of UV polymerization curing conditions on performance of acrylic pressure sensitive adhesives, Macromol. Res. 29 (2021) 129–139, https://doi.org/10.1007/s13233-021-9018-3.
[10] W. Ming, Z. Xie, Z. Jiang, Y. Chen, G. Zhang, Y. Xu, W. He, Progress in optical adhesive and lamination process of touch screen in 3C products, J. Soc. Inf. Disp. 30 (2022) 851–876, https://doi.org/10.1002/jsid.1175.
[11] D. Lee, J. Lee, D. Seo, Y. Jung, H. Lee, D. Kong, S. Song, Backside bonding for extremely narrow bezel at the bottom of flexible displays, J. Soc. Inf. Disp. 32 (2024) 206–215, https://doi.org/10.1002/jsid.1284.
[12] K. Hyun-Sik, H. Hyeon-Deuk, H. Kwan-Young, Ink-step adaptability and reliability of maleimide-functionalized UV-curable optically clear adhesives, Nanosci. Nanotechnol. Lett. 9 (2017) 1146–1152.
[13] P. Majda, J. Skrodzewicz, A modified creep model of epoxy adhesive at ambient temperature, Int. J. Adhes. Adhes. 29 (2009) 396–404, https://doi.org/10.1016/j.ijadhadh.2008.07.010.
[14] S. Mapari, S. Mestry, S.T. Mhaske, Developments in pressure-sensitive adhesives: a review, Polym. Bull. 78 (2021) 4075–4108, https://doi.org/10.1007/s00289-020-03305-1.
[15] D.M. Fitzgerald, Y.L. Colson, M.W. Grinstaff, Synthetic pressure sensitive adhesives for biomedical applications, Prog. Polym. Sci. 142 (2023), https://doi.org/10.1016/j.progpolymsci.2023.101692.
[16] Y. Wu, T. Wang, J. Gao, L. Zhang, J.D.B. Fay, S. Hirth, J. Hankett, Z. Chen, Molecular behavior of 1K polyurethane adhesive at buried interfaces: plasma treatment, annealing, and adhesion, Langmuir 39 (2023) 3273–3285, https://doi.org/10.1021/acs.langmuir.2c03084.
[17] H. Wang, X. Li, E. Zhang, J. Shi, X. Xiong, C. Kong, J. Ren, C. Li, K. Wu, Strong thermo-tolerant silicone-modified waterborne polyurethane/polyimide pressure-sensitive adhesive, Langmuir 39 (2023) 17611–17621, https://doi.org/10.1021/acs.langmuir.3c01564.

[18] Y. Zhang, K. Hasegawa, S. Kamo, K. Takagi, W. Ma, A. Takahara, Enhanced adhesion effect of epoxy resin on metal surfaces using polymer with catechol and epoxy groups, ACS Appl. Polym. Mater. 2 (2020) 1500–1507, https://doi.org/10.1021/acsapm.9b01179.
[19] T. Abe, S. Yamamoto, K. Tanaka, Effect of interfacial local conformation of polymer chains on adhesion strength, Polym. Chem. (2024), https://doi.org/10.1039/d4py00951g.
[20] S. Yamamoto, Y. Tsuji, R. Kuwahara, K. Yoshizawa, K. Tanaka, Effect of condensed water at an alumina/epoxy resin interface on curing reaction, Langmuir 40 (2024) 12613–12621, https://doi.org/10.1021/acs.langmuir.4c01081.
[21] S.W. Lee, J.H. Back, G.S. Shim, S.W. Jang, H.J. Kim, Adhesion performance and optical properties of optically pressure-sensitive adhesives including an isosorbide, Int. J. Adhes. Adhes. 98 (2020), https://doi.org/10.1016/j.ijadhadh.2019.102503.
[22] N. Ballard, Designing acrylic latexes for pressure-sensitive adhesives: a review, Polym. Int. 73 (2024) 75–87, https://doi.org/10.1002/pi.6596.
[23] D. Satas, Handbook of Pressure Sensitive Adhesive Technology, 2nd ed., Van Nostrand Reinhold, New York, 1989.
[24] A.D. O'Donnell, S. Salimi, L.R. Hart, T.S. Babra, B.W. Greenland, W. Hayes, Applications of supramolecular polymer networks, React. Funct. Polym. 172 (2022), https://doi.org/10.1016/j.reactfunctpolym.2022.105209.
[25] H. Jeong, S.J. Hong, J.S. Yuk, H. Lee, H. Koo, S.H. Park, J. Shin, Renewable and degradable triblock copolymers produced via metal-free polymerizations: from low sticky pressure-sensitive adhesive to soft superelastomer, ACS Sustain. Chem. Eng. 11 (2023) 4871–4884, https://doi.org/10.1021/acssuschemeng.3c00312.
[26] K. Boga, A.F. Patti, J.C. Warner, G.P. Simon, K. Saito, Eco-friendly photoreversible adhesives derived from coumarin-functionalized epoxy soybean oil, ACS Appl. Polym. Mater. 5 (2023) 4644–4653, https://doi.org/10.1021/acsapm.3c00091.
[27] S. Wang, W.H. Hu, Y. Nakamura, N. Fujisawa, A.E. Herlyng, M. Ebara, M. Naito, Bio-inspired adhesive with reset-on demand, reuse-many (RORM) modes, Adv. Funct. Mater. 33 (2023), https://doi.org/10.1002/adfm.202215064.
[28] Y.L. Tan, Y.J. Wong, N.W.X. Ong, Y. Leow, J.H.M. Wong, Y.J. Boo, R. Goh, X. J. Loh, Adhesion evolution: designing smart polymeric adhesive systems with on-demand reversible switchability, ACS Nano 18 (2024) 24682–24704, https://doi.org/10.1021/acsnano.4c05598.
[29] D.V. Srinivasan, S. Idapalapati, Review of debonding techniques in adhesively bonded composite structures for sustainability, Sustain. Mater. Technol. 30 (2021), https://doi.org/10.1016/j.susmat.2021.e00345.
[30] Y. Matsumura, K. Yamaoka, R. Ikura, Y. Takashima, Light stimuli-responsive degradable and tough polymeric materials with movable cross-links, ACS Appl. Mater. Interfaces (2025), https://doi.org/10.1021/acsami.5c01169.
[31] K. Ichiwara, Y. Kamo, Y. Suzuki, A. Matsumoto, Thermally-responsive dismantlable adhesion system for steel plates using methacrylate copolymers containing a tert-butoxycarbonyl group, Int. J. Adhes. Adhes. 135 (2024), https://doi.org/10.1016/j.ijadhadh.2024.103846.
[32] M. Iseki, Y. Suzuki, H. Tachi, A. Matsumoto, Design of a high-performance dismantlable adhesion system using pressure-sensitive adhesive copolymers of 2-hydroxyethyl acrylate protected with tert-butoxycarbonyl group in the presence of cross-linker and Lewis acid, ACS Omega 3 (2018) 16357–16368, https://doi.org/10.1021/acsomega.8b02371.
[33] M. Kobayashi, A. Takahara, Environmentally friendly repeatable adhesion using a sulfobetaine-type polyzwitterion brush, Polym. Chem. 4 (2013) 4987–4992, https://doi.org/10.1039/c3py00146f.
[34] Y.L. Rao, A. Chortos, R. Pfattner, F. Lissel, Y.C. Chiu, V. Feig, J. Xu, T. Kurosawa, X. Gu, C. Wang, M. He, J.W. Chung, Z. Bao, Stretchable self-healing polymeric dielectrics cross-linked through metal-ligand coordination, J. Am. Chem. Soc. 138 (2016) 6020–6027, https://doi.org/10.1021/jacs.6b02428.
[35] H. Park, T. Kang, H. Kim, J.C. Kim, Z. Bao, J. Kang, Toughening self-healing elastomer crosslinked by metal–ligand coordination through mixed counter anion dynamics, Nat. Commun. 14 (2023), https://doi.org/10.1038/s41467-023-40791-z.
[36] X. Wu, J. Wang, J. Huang, S. Yang, Robust, stretchable, and self-healable supramolecular elastomers synergistically cross-linked by hydrogen bonds and coordination bonds, ACS Appl. Mater. Interfaces 11 (2019) 7387–7396, https://doi.org/10.1021/acsami.8b20303.
[37] R.K. Bose, N. Hohlbein, S.J. Garcia, A.M. Schmidt, S. Van Der Zwaag, Connecting supramolecular bond lifetime and network mobility for scratch healing in poly (butyl acrylate) ionomers containing sodium, zinc and cobalt, Phys. Chem. Chem. Phys. 17 (2015) 1697–1704, https://doi.org/10.1039/c4cp04015e.
[38] S. Thanneeru, S.S. Duay, L. Jin, Y. Fu, A.M. Angeles-Boza, J. He, Single chain polymeric nanoparticles to promote selective hydroxylation reactions of phenol catalyzed by copper, ACS Macro Lett. 6 (2017) 652–656, https://doi.org/10.1021/acsmacrolett.7b00300.
[39] H. Murakami, K. Futashima, M. Nanchi, S. Kawahara, Unique thermal behavior of acrylic PSAs bearing long alkyl side groups and crosslinked by aluminum chelate, Eur. Polym. J. 47 (2011) 378–384, https://doi.org/10.1016/j.eurpolymj.2010.12.012.
[40] Y.A. Chen, R.H. Lai, W.C. Lin, H.Y. Huang, S.J. Chen, C.M. Yeh, H.L. Huang, M. M. Elsenety, C.C. Hu, C.H. Yu, H.H. Chou, Enhancing self-healing and mechanical robustness through aluminum acetylacetonate-driven metal-ligand coordination for skin-inspired sensing, ACS Appl. Polym. Mater. 6 (2024) 6976–6987, https://doi.org/10.1021/acsapm.4c00545.
[41] E. Khare, N. Holten-Andersen, M.J. Buehler, Transition-metal coordinate bonds for bioinspired macromolecules with tunable mechanical properties, Nat. Rev. Mater. 6 (2021) 421–436, https://doi.org/10.1038/s41578-020-00270-z.
[42] Y. Miwa, J. Kurachi, Y. Sugino, T. Udagawa, S. Kutsumizu, Toward strong self-healing polyisoprene elastomers with dynamic ionic crosslinks, Soft Matter 16 (2020) 3384–3394, https://doi.org/10.1039/d0sm00058b.
[43] R. Ikura, S. Murayama, J. Park, Y. Ikemoto, M. Osaki, H. Yamaguchi, A. Harada, G. Matsuba, Y. Takashima, Fabrication and mechanical properties of knitted dissimilar polymeric materials with movable cross-links, Mol. Syst. Des. Eng. 7 (2022) 733–745, https://doi.org/10.1039/d2me00016d.
[44] J. Sawada, D. Aoki, H. Otsuka, T. Takata, A guiding principle for strengthening crosslinked polymers: synthesis and application of mobility-controlling rotaxane crosslinkers, Angew. Chem. Int. Ed. 58 (2019) 2765–2768, https://doi.org/10.1002/anie.201813439.
[45] S. Ando, K. Ito, Recent progress and future perspective in slide-ring based polymeric materials, Macromolecules (2025), https://doi.org/10.1021/acs.macromol.4c02021.
[46] K. Kato, M. Naito, K. Ito, A. Takahara, K. Kojio, Freestanding tough glassy membranes produced by simple solvent casting of polyrotaxane derivatives, ACS Appl. Polym. Mater. 3 (2021) 4177–4183, https://doi.org/10.1021/acsapm.1c00622.
[47] Y. Qian, S. Kosaba, R. Ikura, K. Yamaoka, Y. Takashima, Design of functional and stable adhesion systems using reversible and movable crosslinked materials, Polym. J. (2025), https://doi.org/10.1038/s41428-024-01011-7.
[48] S. Kawano, K. Nakano, H. Sato, M. Muraoka, M. Shizuma, Photo- and thermo-responsive supramolecular polymer networks via in situ polymerization using homoternary macrocyclic host with coumarin monomers in water, Polym. Chem. 13 (2022) 5820–5828, https://doi.org/10.1039/d2py00952h.
[49] K.V. Dikshit, A.M. Visal, F. Janssen, A. Larsen, C.J. Bruns, Pressure-sensitive supramolecular adhesives based on lipoic acid and biofriendly dynamic cyclodextrin and polyrotaxane cross-linkers, ACS Appl. Mater. Interfaces 15 (2023) 17256–17267, https://doi.org/10.1021/acsami.3c00927.
[50] S. Kawano, K. Ichiwara, H. Taneichi, S. Hamada, Y. Fujino, O. Shimomura, M. Shizuma, Hydrophobic cyclodextrin dimer-assisted self-healing elastomer: movable crosslinks of pseudo-rotaxane with recyclable and separable functionality, RSC Appl. Polym. (2024), https://doi.org/10.1039/d4lp00196f.
[51] S. Kosaba, R. Ikura, K. Yamaoka, T. Arai, Y. Takashima, Recyclable tough adhesive sheets with movable cross-links for sustainable use, ACS Appl. Mater. Interfaces 16 (2024) 25393–25403, https://doi.org/10.1021/acsami.4c03806.
[52] M.B. Yi, T.H. Lee, G.Y. Han, H. Kim, H.J. Kim, Y. Kim, H.S. Ryou, D.U. Jin, Movable cross-linking in adhesives: superior stretching and adhesion properties via a supramolecular sliding effect, ACS Appl. Polym. Mater. 3 (2021) 2678–2686, https://doi.org/10.1021/acsapm.1c00240.
[53] Y. Kawai, J. Park, S. Murayama, R. Ikura, M. Osaki, T. Konishi, G. Matsuba, Y. Takashima, Hybridizing a dual-cross network and a linear glassy polymer for dynamic contributions to high mechanical toughness based on phase-separated structures, Macromolecules 56 (2023) 4503–4512, https://doi.org/10.1021/acs.macromol.3c00178.
[54] C.A. Dahlquist, Adhesion: Fundamental and Practice, McLaren, London, 1966.
[55] M.M. Feldstein, E.V. Bermesheva, Y.C. Jean, G.P. Misra, R.A. Siegel, Free volume, adhesion, and viscoelastic properties of model nanostructured pressure-sensitive adhesive based on stoichiometric complex of poly(N-vinyl pyrrolidone) and poly (ethylene glycol) of disparate chain lengths, J. Appl. Polym. Sci. 119 (2011) 2408–2421, https://doi.org/10.1002/app.32917.
[56] S. Ponce, J. Bico, B. Roman, Effect of friction on the peeling test at zero-degrees, Soft Matter 11 (2015) 9281–9290, https://doi.org/10.1039/c5sm01203a.
[57] V.A. Inozemtsev, A.L. Gamov, A.P. Moscalets, Soft to tough: ordering in and tack of polymeric materials, Soft Matter 14 (2018) 2184–2193, https://doi.org/10.1039/c7sm02273e.
[58] P. Elzière, C. Dalle-Ferrier, C. Creton, É. Barthel, M. Ciccotti, Large strain viscoelastic dissipation during interfacial rupture in laminated glass, Soft Matter 13 (2017) 1624–1633, https://doi.org/10.1039/c6sm02785g.
[59] C.Y. Hui, Z. Liu, H. Minsky, C. Creton, M. Ciccotti, Mechanics of an adhesive tape in a zero degree peel test: effect of large deformation and material nonlinearity, Soft Matter 14 (2018) 9681–9692, https://doi.org/10.1039/c8sm01731j.
[60] Michiko Yamanaka, Michael D. Determan, Albert I. Everaerts, Thu-Van T. Tran, Jayshree Seth, Stretch releasable pressure-sensitive adhesive tape, US 8,557,378 B2. https://patentimages.storage.googleapis.com/16/ab/b6/4e4c48d0354604/US8557378.pdf, 2013. (Accessed 30 September 2025).
[61] G.R. Hamed, C.H. Shieh, Relationship between the cohesive strength and the tack of elastomers, J. Polym. Sci. Part A-2 Polym. Phys. 21 (1983) 1415–1425, https://doi.org/10.1002/pol.1983.180210812.
[62] C. Creton, L. Leibler, How does tack depend on time of contact and contact pressure? J. Polym. Sci. B Polym. Phys. 34 (1996) 545–554, https://doi.org/10.1002/(SICI)1099-0488(199602)34:3<545::AID-POLB13>3.0.CO;2-I.
[63] I.K. Mohammed, M.N. Charalambides, A.J. Kinloch, Modelling the interfacial peeling of pressure-sensitive adhesives, J. Nonnewton Fluid Mech. 222 (2015) 141–150, https://doi.org/10.1016/j.jnnfm.2014.10.005.